doi:10.1016/j.jmb.2004.07.067 J. Mol. Biol. (2004) 342, 861–875

JMB

Available online at www.sciencedirect.com

SCIENCE DIRECT®

ELSEVIER

Structure and Function of a Regulated Archaeal Triosephosphate Isomerase Adapted to High Temperature

Helen Walden[1], Garry L. Taylor[1]*, Esben Lorentzen[2], Ehmke Pohl[2] Hauke Lilie[3], Alexander Schramm[4], Thomas Knura[4], Kim Stubbe[4] Britta Tjaden[4] and Reinhard Hensel[4]*

[1]*Centre for Biomolecular Sciences, University of St Andrews, St Andrews, Fife KY16 9ST, Scotland, UK*

[2]*European Molecular Biology Laboratory, Hamburg Outstation, Notkestr. 85 D-22603 Hamburg, Germany*

[3]*Institut für Biotechnologie Universität Halle-Wittenberg Kurt-Mothes-Str. 3, D-06099 Halle, Germany*

[4]*FB9 Mikrobiologie, Universität Duisburg-Essen Universitätsstr. 5, D-45117 Essen, Germany*

**Corresponding authors*

Triosephophate isomerase (TIM) is a dimeric enzyme in eucarya, bacteria and mesophilic archaea. In hyperthermophilic archaea, however, TIM exists as a tetramer composed of monomers that are about 10% shorter than other eucaryal and bacterial TIM monomers. We report here the crystal structure of TIM from *Thermoproteus tenax*, a hyperthermophilic archaeon that has an optimum growth temperature of 86 °C. The structure was determined from both a hexagonal and an orthorhombic crystal form to resolutions of 2.5 Å and 2.3 Å, and refined to *R*-factors of 19.7% and 21.5%, respectively. In both crystal forms, *T. tenax* TIM exists as a tetramer of the familiar $(\beta\alpha)_8$-barrel. In solution, however, and unlike other hyperthermophilic TIMs, the *T. tenax* enzyme exhibits an equilibrium between inactive dimers and active tetramers, which is shifted to the tetramer state through a specific interaction with glycerol-1-phosphate dehydrogenase of *T. tenax*. This observation is interpreted in physiological terms as a need to reduce the build-up of thermolabile metabolic intermediates that would be susceptible to destruction by heat. A detailed structural comparison with TIMs from organisms with growth optima ranging from 15 °C to 100 °C emphasizes the importance in hyperthermophilic proteins of the specific location of ionic interactions for thermal stability rather than their numbers, and shows a clear correlation between the reduction of heat-labile, surface-exposed Asn and Gln residues with thermoadaptation. The comparison confirms the increase in charged surface-exposed residues at the expense of polar residues.

Keywords: hyperthermophile; thermostability; thermoadaptation; triosephosphate isomerase; *Thermoproteus tenax*

Introduction

The lifestyle of hyperthermophilic organisms growing in habitats of temperatures exceeding 80 °C, and sometimes in excess of 100 °C, arouses curiosity about the molecular adaptation that guarantees adequate stability and function of the cell constituents under these extreme conditions. Given the potential biotechnological applications of proteins resistant to heat-denaturation, the major focus of research has been an attempt to discover the structural determinants of protein thermostability. Over the last decade, several comparative analyses of crystal structures of homologous proteins from organisms with different optimal growth temperatures have been performed,[1–8] uncovering an unexpected diversity of adaptation mechanisms of the various proteins.[9–11] Almost without exception, the structural differences between homologous proteins from mesophiles and thermophiles have been interpreted simply

Abbreviations used: GLPDH, glycerol-1-phosphate dehydrogenase; TIM, triosephosphate isomerase; DHAP, dihydroxyacetone phosphate; GAP, glyceraldehyde 3-phosphate; EMP, Embden–Meyerhof–Parnas; PGK, 3-phosphoglycerate kinase; FBPA, fructosebisphosphate aldolase; GAPDH, glyceraldehyde-3-phosphate dehydrogenase; GAPN, non-phosphorylating glyceraldehyde-3-phosphate dehydrogenase.

E-mail addresses of the corresponding authors: glt2@st-andrews.ac.uk; r.hensel@uni-essen.de

with respect to thermodynamic and kinetic thermostability. However, other aspects of thermoadaptation, such as the need to guarantee adequate function at high temperature and the interaction with the intracellular milieu of the thermophilic cell, have largely been neglected. The comparative studies have shown that in some but not all proteins analyzed, the number of ionic interactions increases with increasing temperature, especially at the upper range of the temperature scale, the number of internal cavities decreases, and the proportion of secondary structure increases, reflecting the requirement for a more compact and rigid conformation stabilizing the protein against heat-denaturation. A further striking observation is that some proteins from hyperthermophilic organisms exist in a higher oligomeric state than their mesophilic counterparts, suggesting that the additional subunit interactions support the stability of the whole molecule under extreme conditions. The more stringent conditions in the upper temperature range also result in changes of amino acid composition in some proteins, such as an increase in charged residues and a decrease in labile residues, e.g. asparagine, glutamine and cysteine, especially at the surface of the protein. Most of these rather general structural properties do not change uniformly in all proteins with adaptation to high temperature. Only the increase of charged, sufaceexposed residues at the expense of polar residues seems to represent an obligate trend in thermoadaptation.[12] For a full understanding of the molecular principles of thermoadaptation, further detailed analyses of the structural background of intrinsic stability are necessary, which must be complemented by studies considering the individual demands for specific catalytic and regulatory properties of proteins in the thermophilic cell, including the intracellular milieu conditions influencing both their stability and function *in vivo*.

For several reasons, triosephosphate isomerase (TIM) represents an ideal candidate for studies of protein thermoadaptation. TIM catalyses the interconversion of dihydroxyacetone phosphate (DHAP) and D-glyceraldehyde 3-phosphate (GAP) within the Embden–Meyerhof–Parnas (EMP) pathway,[13] and is ubiquitous in nature. It has been characterised extensively both structurally and biochemically. Three-dimensional structures of TIMs from psychrophilic,[14] mesophilic[15–18] moderately thermophilic[19,20] and hyperthermophilic[1,4] organisms are known, thus allowing a comparative structural analysis across a broad temperature range of 15–100 °C.

The two hyperthermophile crystal structures of TIMs are from the bacterium *Thermotoga maritima* (optimal temperature (T_{opt}) 80 °C) and the archaeon *Pyrococcus woesei* (T_{opt} 100 °C).[1,4] Whereas eucaryal, bacterial and archaeal TIMs adapted to lower temperatures are homodimers, the hyperthermophilic TIMs are tetrameric.[21,22] The TIM of *T. maritima* (TmTIM) exists as a bifunctional fusion protein *in vivo*, with the N terminus of TmTIM linked covalently to the C terminus of 3-phosphoglycerate kinase (PGK). The wild-type protein is tetrameric, comprising four PGK-TIM chains linked covalently through disulphide bonds.[23]

Here, we report the crystal structure of TIM from *Thermoproteus tenax* (TtxTIM), a hyperthermophilic archeon with T_{opt} 86 °C. In contrast to the TIMs of *T. maritima*, *Methanothermus fervidus* or *P. woesei*, TtxTIM does not form stable tetramers, but exists in a dimer/tetramer equilibrium. This observation prompted us to analyze the structural basis for the weaker tetrameric association in more detail, and to focus on the biochemical and functional properties of TxTIM. Our results suggest that specific functional requirements, dictated by the physiology at high temperature, influence the mechanisms of protein thermostabilisation significantly, thereby expanding our appreciation of the various factors involved in thermoadaptation.

Results

Structure of the TtxTIM

Deduced primary structure

The TtxTIM gene comprises 678 bp and codes for 226 residues (Figure 1). Like other archaeal TIMs, independent of their mesophilic or thermophilic origin, the *T. tenax* enzyme with a molecular mass of 23.3 kDa is approximately 10% smaller than that of the eucaryal and bacterial counterparts. Also common to all archaeal TIMs analyzed to date, there is a low level of sequence similarity with the eucaryal and bacterial enzymes (20–25% identity).

Spatial structure

Two crystal forms of TtxTIM were obtained: a hexagonal crystal form of the apo-enzyme in 50 mM Hepes–KOH (pH 7.5), 0.8 M sodium potassium phosphate and an orthorhombic crystal form of the binary 2-carboxyethylphosphonic acid/TIM complex in 0.1 M sodium acetate (pH 4.6), 0.2 M ammonium sulfate, 20–30% (w/v) PEG 4000 (Table 1). Both crystal forms are in the closed conformation, providing a good basis for comparisons with the other known TIM structures. Within the asymmetric unit of both crystal forms there are two homotetramers, ABCD and EFGH. Each tetramer comprises a dimer of classical TIM dimers, AB and CD in one tetramer, EF and GH in the other. The orthorhombic crystal form is used in the analysis due to the higher resolution of the data. The TtxTIM structures in the hexagonal and orthorhombic forms are very similar, having an rms difference of 0.2 Å, with the exception of the dimer interface residues 66–69, which have an rms difference of 0.6 Å.

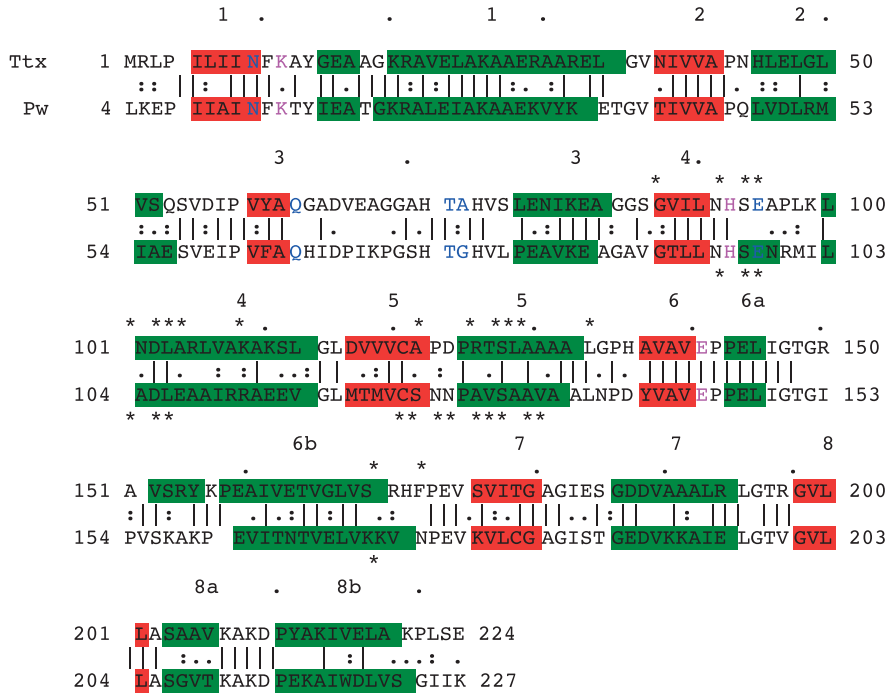

Figure 1. Structural alignment of TtxTIM and PwTIM sequences. Strands are marked in red, helices in green, catalytic residues in magenta and conserved dimer interface residues in blue. The residues marked with an asterisk are involved in the tetramer interface of each TIM.

Monomeric structure

Each subunit of TtxTIM displays the same fold as the other TIMs. Figure 1 shows a sequence alignment of the TtxTIM and the *P. woesei* TIM (PwTIM). The two archaeal TIMs share 52% sequence identity, which is reflected in the rms difference between the C^{α} atoms of the two TIMs of 0.97 Å. This is compared to the lowest rms difference of 1.72 Å when comparing the PwTIM with any of the other TIMs. Surprisingly, the sequence comparison between TtxTIM and PwTIM shows that many of the non-conservative substitutions occur within the tetramer interface

Table 1. Summary of the X-ray data and refinement statistics for the two TtxTIM crystal forms

	Crystal	
	Hexagonal	Orthorhombic
Spacegroup	$P6_522$	$P2_12_12$
Resolution (Å)	30–2.5	16.2–2.3
No. observations	440,620	582,128
No. unique reflections	99,570	86,753
Completeness (%)	97.2 (98.3)	97.9 (99.2)
R_{merge} (%)[a]	5.8 (36.4)	10.4 (23.1)
$\langle I/\sigma(I)\rangle$	20.8 (3.4)	6.8 (2.6)
R-factor (%)	19.7	21.5
R_{free}(%)	22.6	25.9
rmsd from ideality		
Bond lengths (Å)	0.005	0.011
Bond angles (deg.)	1.282	1.651
Number of atoms		
Protein	13,007	13,005
Ligand	32	72
Water	711	459
Average *B*-factors (Å^2)		
Protein (chain)	31.0(A), 34.6(B), 26.4(C), 29.7(D), 35.2(E), 43.7(F), 54.9(G), 46.3(H)	13.1(A), 17.0(B), 14.6(C), 16.6(D), 18.6(E), 21.5(F), 25.5(G), 28.8(H)
Ligand	38.6	18.4
Water	34.1	19.2

Numbers in parentheses refer to the highest-resolution shell.

[a] $R_{merge} = \sum |I(k) - \langle I\rangle| / \sum I(k)$, where $I(k)$ is the value of the kth measurement of the intensity of a reflection, $\langle I\rangle$ is the mean value of the intensity of that reflection, and the summation is of all the measurements.

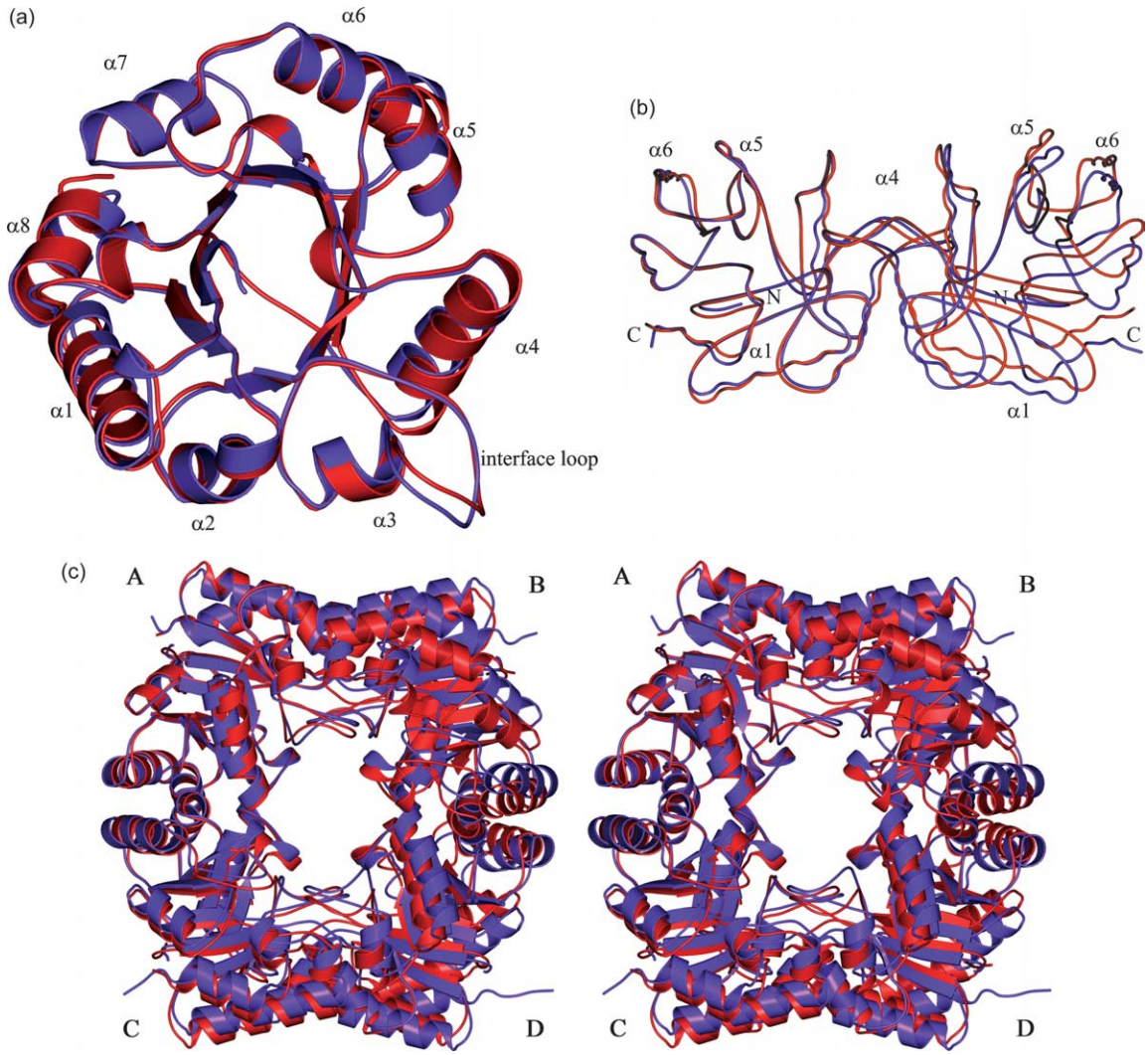

Figure 2. Superposition of the TtxTIM (purple) and PwTIM (red). (a) Superposition of the monomers with the α-helices and dimer interface loop labeled. (b) Superposition of the classical TIM dimer, each as an C^{α} trace. (c) A stereo diagram of the TtxTIM and PwTIM tetramers superimposed, showing the twist in the TtxTIM tetramer interface.

helices, and in the loop following β3, which is the dimer interface loop. The levels of secondary structure are comparable, with TtxTIM having 59.7% of its residues involved in secondary structure elements compared to 59.5% of PwTIM residues. The monomeric structures are highly superimposable, with the β-strands being very similar, but there are some differences in some of the loops and the helices (Figure 2(a)).

The N terminus of the PwTIM is fixed to the core of the barrel *via* an ion-pair. This is not conserved in the TtxTIM, although the TtxTIM N terminus also points back into the core of the barrel, but not to the same extent as the PwTIM. The C-terminal end of helix 4 is closer to the core of the barrel in the TtxTIM, but the C-terminal end of helix 6 is further from the core in the TtxTIM. Both these helices are involved in the tetramer association. However, the TtxTIM helix 4 does not have either of the ion-pair networks seen in the PwTIM. The other major point of difference between the two hyperthermophilic archaeal TIMs is in the dimer interface loop, which has swung 2.1 Å from the PwTIM at the farthest point. The two archaeal TIMs are also similar in size, with monomeric volumes of 26,700 $Å^3$ and 27,300 $Å^3$, dimeric volumes of 55,000 $Å^3$ and 56,500 $Å^3$, and tetrameric volumes of 113,200 and 114,400 $Å^3$ for TtxTIM and PwTIM, respectively.

Dimer association

The conformation of the classical TIM dimer is different in the TtxTIM compared to both the more thermostable PwTIM and the less thermostable TIMs (Figure 2(b)).

There is an obvious shift in the position of the second monomer, which is not seen in any of the other TIMs. It is not clear how this shift is achieved, as, although there are differences in the chemical nature of the exposed surface area between the TtxTIM and all the other TIMs (Table 2), there are also differences between PwTIM and the other TIMs and yet the dimer conformation is essentially identical.[1] A key difference in the dimerisation of

Table 2. Subunit volumes, accessible surface area (*ASA*) of monomers and oligomers, and the nature of the exposed surface area of TIMs adapted to various temperatures

TIM	Vm (15 °C)	Ye (37 °C)	Bs (65 °C)	*T*m (80 °C)	Ttx (86 °C)	Pw (100 °C)
Monomer volume (Å^3)	31,100	30,800	30,800	33,000	26,700	27,300
ASA (Å^2)	11,130	11,300	10,700	11,900	10,100	9900
% Buried	46.0	45.6	49.3	42.3	42.3	45.0
% Exposed charged	42.5	44.9	39.9	52.0	47.7	52.0
% Polar	22.6	28.8	27.4	20.4	19.0	18.5
% Hydrophobic	27.7	20.8	25.9	21.1	27.3	27.3
Dimer volume (Å^3)	63,800	64,100	63,700	68,900	55,000	56,500
ASA (Å^2)	18,900	19,300	17,800	20,200	17,200	17,100
% Buried	49.0	49.4	53.4	47.2	47.7	48.9
% Exposed charged	45.2	48.3	44.2	56.2	54.2	54.1
% Polar	23.0	26.6	27.5	19.8	15.8	14.4
% Hydrophobic	24.2	19.6	21.7	17.5	24.8	27.4
Tetramer volume (Å^3)	–	–	–	140,600	113,200	114,400
ASA (Å^2)	–	–	–	38,200	31,400	31,400
% Buried	–	–	–	47.9	50.3	50.6
% Exposed charged	–	–	–	56.1	58.2	57.4
% Polar	–	–	–	19.4	14.1	15.4
% Hydrophobic	–	–	–	18.0	22.0	22.7

The optimal growth temperature of each organism is given in parentheses. Abbreviations: Vm, *Vibrio marinus*; Ye, yeast; Bs, *B. stearothermophilus*, Tm, *T. maritima*, Ttx, *T. tenax*, Pw, *P. woesei*.

TtxTIM compared to the PwTIM is in the burial of hydrophobic residues. The PwTIM shows no change in the proportion of hydrophobic surface area exposed on formation of the dimer, whereas the dimerisation of the TtxTIM decreases the amount of hydrophobic exposed surface area from 27.3% to 24.8%. This is comparable to the burial of hydrophobic surface area upon dimerisation of the less thermostable TIMs.

Tetramer association

The TtxTIM tetramer is also arranged as a dimer of classical dimmers, as seen in the PwTIM tetramer (Figure 2(c)),[1] and in common with the PwTIM tetramer, there is no evidence of ion pairs across the interface, the tetramer being stabilized predominantly by hydrophobic interactions across residues in helices 4, 5 and 6, and the loops linking them. There are 17 residues from each TtxTIM monomer involved in the interface compared to 16 from each PwTIM monomer. Of the interface residues, 13 are in equivalent positions and, of those, only four are conserved completely (Figure 1). These sequence changes give rise to a slightly less hydrophobic interface in TtxTIM (40% polar and 61% hydrophobic) compared to the PwTIM (31% polar and 69% hydrophobic). The TtxTIM has a more extensive interface than the PwTIM, with 9.6% of each monomer contributing to a total interface accessible surface area of 900 Å^2. This is in comparison with 700 Å^2 in the PwTIM, only 7.6% of each monomer.

Electrostatic interactions

TtxTIM does not show any significant difference in the number of ion-pairs, either intramolecular or intermolecular, when compared with the PwTIM or the other TIMs. The only TIM that has a significantly higher number of ion-pairs is the hyperthermophilic *T. maritima* TIM. It is clear that the archaeal representatives of the TIM family do not exploit ion-pairs as a means of achieving thermoadaptation. In contrast with the PwTIM, TtxTIM does not lack the "conserved" salt-bridge seen in all the other TIMs.[4] Although not in exactly the same place as in the other TIMs, TtxTIM has an ion-pair network between Arg154, Glu183 and Asp187, which serves to tether helices 6 and 7 to each other, as in the other TIMs. However, TtxTIM does lack some of the unique ion-pairs seen in the PwTIM structure: the pair linking the N terminus to the core of the barrel is lost, as are both of the networks found in helix 4. It does have the ion-pair responsible for tethering the two sections of helix 6 to each other, Glu144 and Lys156. Despite a lack of a role for ion-pairs in the stabilisation of the hyperthermophilic TIMs, it is interesting to note that the three most stable TIMs: TmTIM, TtxTIM and PwTIM, all have more charged exposed surface area than any of the less thermostable TIMs, at the expense of polar residues (Figure 3).

Deamidation

The apparent correlation of increased thermostability with a decrease in the amount of exposed polar surface area is mirrored by a decrease in the number of polar residues in thermophilic genomes.[12] Given the susceptibility of asparagine to deamidation, and to a tenfold lesser extent glutamine, it is possible that surface-exposed Asn and Gln residues are more susceptible to deamidation than buried ones. Consequently, a possible mechanism for thermostabilisation is to reduce the number of surface-exposed Asn/Gln residues, or to protect them from deamidation. Using the criteria outlined in Materials and Methods, all of

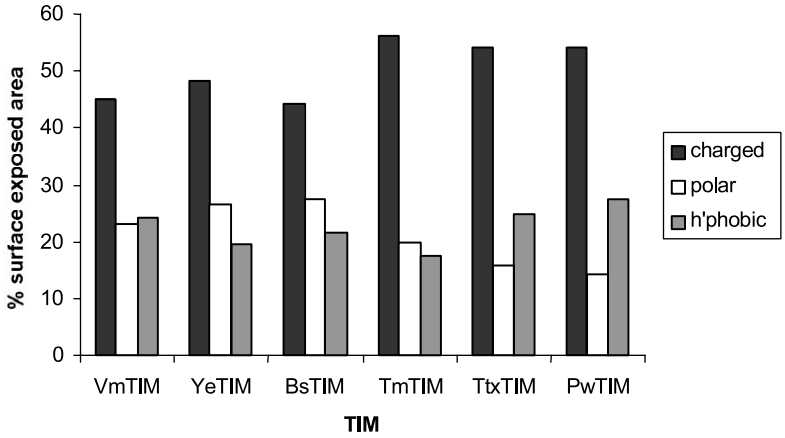

Figure 3. The graph shows the nature of the exposed surface area in each classical TIM dimer.

the Asn and Gln residues that fulfill both criteria 1 and 2 are solvent-accessible (Table 3). With adaptation to the upper temperature range there is a decrease in the total number of surface-exposed Asn and Gln residues, especially in the number of amidated residues with preferred susceptibility to deamidation (fulfilling both criteria).

Biochemical and enzymic properties of TtxTIM

Oligomerisation state of TtxTIM under non-denaturing conditions

Determination of the sedimentation equilibrium by analytical ultracentrifugation with protein solutions of 5 to 500 μg/ml of recombinant TtxTIM showed the existence of a rapid equilibrium reaction between dimers and tetramers with molecular masses of 46,600 Da or 93,000 Da, respectively (Figure 4). Analysis of the apparent molecular mass of the protein as a function of total protein concentration at 25 °C yielded K_D values of $7(\pm 2)\times 10^{-8}$ M. Dilution-dependent inactivation of enzyme solutions gave hints that dimers and tetramers differ regarding their enzymatic activity. For a more defined correlation between oligomeric state and enzyme activity, a stock solution of 0.5 mg/ml of recombinant TtxTIM was diluted to 1 μg/ml at 25 °C and the activity was tested over the course of two hours. As shown in Figure 4, the concentration-dependence of the average molecular mass as deduced from the sedimentation equilibrium centrifugation experiments, and the concentration-dependence of the residual enzyme activity of the various enzyme solutions coincides very well, indicating that dimeric TtxTIM is virtually inactive. As a confirmation for the reversibility of dissociation, a re-concentration of a 10 μg/ml solution, with 71% residual activity, back to the initial concentration of 0.5 mg/ml resulted in a full restoration of activity.

Kinetic parameters of the tetrameric TtxTIM

K_m and V_{max} values for both directions of the enzyme reaction were determined only at 70 °C, i.e. 16 deg. C below the physiological optimum, in order to avoid rapid heat-destruction of the labile substrates.[22] The K_m values for DHAP and GAP (calculated for the reactive (unhydrated) substrate,

Table 3. Solvent-accessible asparagine and glutamine residues and their susceptibility to deamidation in TIMs adapted to different temperatures

TIM	Vm (15 °C)	Ye (37 °C)	Bs (65 °C)	Tm (80 °C)	Ttx (86 °C)	Pw (100 °C)
A. *Asparagine*						
Residues/monomer	12	12	5	6	6	8
SA	6	5	2	1	1	2
Susceptible (1)[a]	3	8	3	1	2	2
SA and susceptible (1)[a]	3	5	2	1	1	2
Susceptible (1+2)[a]	2	5	1	0	1	0
SA and susceptible (1+2)[a]	2	5	1		1	
B. *Glutamine*						
Residues/monomer	8	7	14	8	2	2
SA	5	2	9	4	1	0
Susceptible (1)[a]	7	4	8	3	1	0
SA and susceptible (1)[a]	4	2	6	3	1	
Susceptible (1+2)[a]	4	2	5	1	1	0
SA and susceptible (1+2)[a]	4	2	5	1	1	

The optimal growth temperature for each organism is indicated. *SA*, solvent accessible. For abbreviations of organisms, see the legend to Table 2.

[a] 1 and 2 refer to the criteria outlined in the Structure analysis section of Materials and Methods.

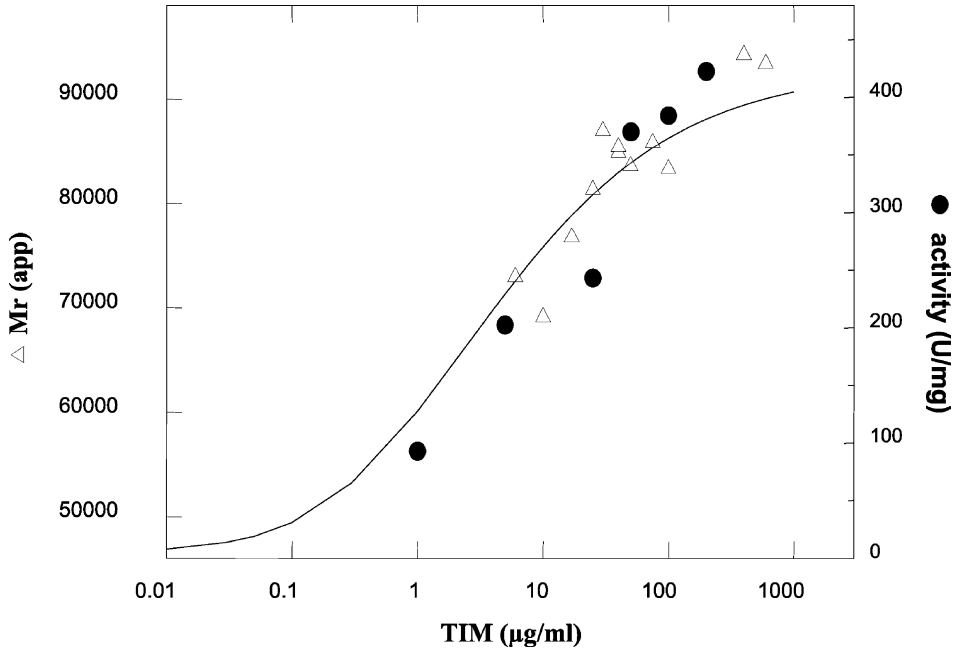

Figure 4. Average molecular mass and specific activity of TIM solutions as a function of protein concentration at 25 °C. Average molecular mass was determined by sedimentation equilibrium centrifugation. Specific activity (enzyme assay at 35 °C) was determined after equilibrating the protein solution over two hours at the given concentration. Data were fit according to equation (1) (see Materials and Methods).

which is present at 17.6% at 70 °C)[24] have been determined to be 0.9 mM and 0.2 mM, respectively. Like other mesophilic or thermophilic TIMs, TxTIM exhibits a significantly higher V_{max} for the GAP/DHAP isomerization (6200 units/mg; auxiliary enzyme: *M. thermautotrophicus* GLPDH) as compared to the reverse reaction (2000 units/mg; auxiliary enzyme: *T. tenax* GAPN). Using *T. tenax* GLPDH instead of *M. thermautotrophicus*GLPDH as auxiliary enzyme for the GAP/DHAP isomerization, V_{max} increases even to 9500 units/mg indicating a specific interaction between both *T. tenax* enzymes.

Reversible and irreversible inactivation of TtxTIM influenced by temperature, proteins and low molecular mass compounds

A tenfold dilution of a freshly prepared 0.5 mg/ml of TtxTIM solution incubated at temperatures from 5 °C to 80 °C, resulted in a decrease of activity down to 55–65% residual activity with a very similar time-course of inactivation over the whole temperature range (Figure 5). Also evident in Figure 5, the final activity as determined after two hours of incubation at the respective temperature decreases only slightly up to 80 °C. The similar time-course of inactivation over the given temperature range suggests that at higher temperatures, where no appropriate molecular mass determinations are possible, respective changes of the oligomeric state of the TtxTIM (i.e. dissociation to dimers) would be responsible for the observed deactivation. We cannot exclude the possibility, however, that the dimers become active at higher temperatures and thus compensate the loss in activity resulting in that rather unexpected minor temperature dependence of deactivation. Some confirmation that dissociation into dimers is due to the observed deactivation in the temperature range up to 80 °C, is that at 80 °C the inactivation is reversible showing a 100% return of activity after cooling down to room temperature and concentrating the sample up to 0.5 mg/ml.

Interestingly, the reversible deactivation of TtxTIM is hindered or even prevented completely by the presence of GLPDH. As shown in Figure 6, the addition of recombinant *M. thermautotrophicus* GLPDH results in an approximate 95% stabilisation of the activity at 80 °C, and the addition of the *T. tenax* GLPDH completely stabilizes the TtxTIM activity. In contrast, no effect could be observed with hen egg-white lysozyme or other *T. tenax* enzymes such as fructosebisphosphate aldolase (FBPA), glyceraldehyde-3-phosphate dehydrogenase (GAPDH) or non-phosphorylating glyceraldehyde-3-phosphate dehydrogenase (GAPN). This suggests a specific interaction of TtxTIM with GLPDH, particularly with the *T. tenax* enzyme. Low molecular mass solutes such as glycerol, inositol, trehalose, KCl, K_2HPO_4, K_2SO_4 at concentrations of 100 mM are not able to prevent the reversible inactivation of TtxTIM.

Above 85 °C, the inactivation kinetics become more complex. As shown in Figure 7, at 92 °C, an initial fast inactivation reaction ($t_{0.5} \approx$ two minutes), which is probably due to dissociation, is followed by a slower decrease of activity ($t_{0.5} = 45$ minutes). After cooling and concentration of a sample inactivated to 5% residual activity, no reactivation

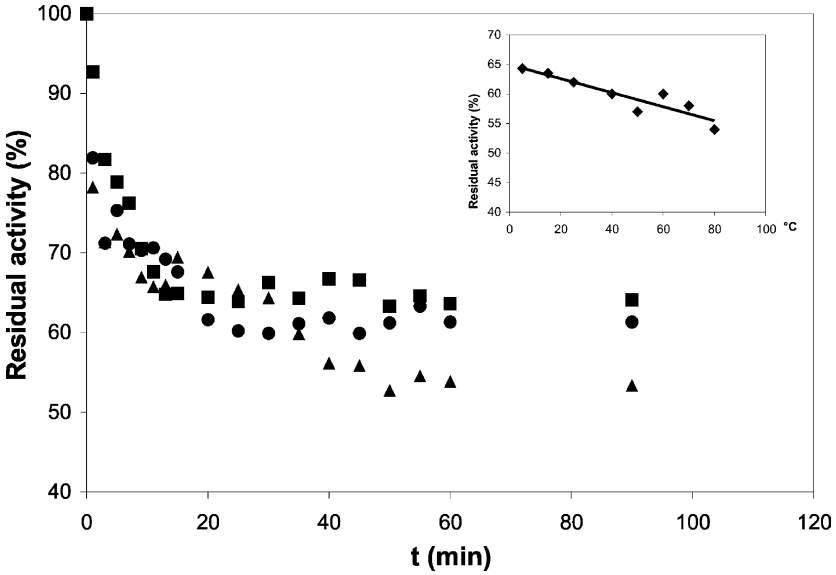

Figure 5. Reversible inactivation of TtxTIM at temperatures of 5 °C-80 °C. The time-course of reversible inactivation of a freshly prepared 50 μg/ml solution is shown for 5 °C (■), 25 °C (●) and 80 °C (▲). The final specific activities reached after two hours of incubation at the respective temperature is given in the inset.

could be observed, indicating that irreversible denaturation occurs, probably in the course of the second, slower inactivation reaction.

A search for compounds protecting the enzyme against irreversible thermal denaturation led to the observation that trehalose, which is present in *T. tenax* at concentrations of approximately 60 mM,[25] prevents the second, slow inactivation reaction. Addition of 100 mM trehalose to the TIM solution resulted in an activity decrease of only 60%, similar to the activity level reached at temperatures below 85 °C (Figure 6) and allowed a 100% return of the activity upon a reconcentration of the solution to 0.5 mg/ml. Other solutes such as KCl, NH_4SO_4 and cyclic 2,3-diphosphoglycerate[26] are less efficient (Figure 7) or in the case of K_2SO_4, glycerine and di-myo-inositol-1,1′-phosphate, not at all active in stabilizing the enzyme.[27]

Discussion

The investigations on TtxTIM suggest that more detailed studies are necessary to differentiate between the various structural prerequisites of thermoadaptation, and that factors other than just structure need to be considered for a full understanding of protein stability and function at high temperature.

The contribution of electrostatic interactions to thermostability is highlighted in this study. Although there is no direct numerical trend in the

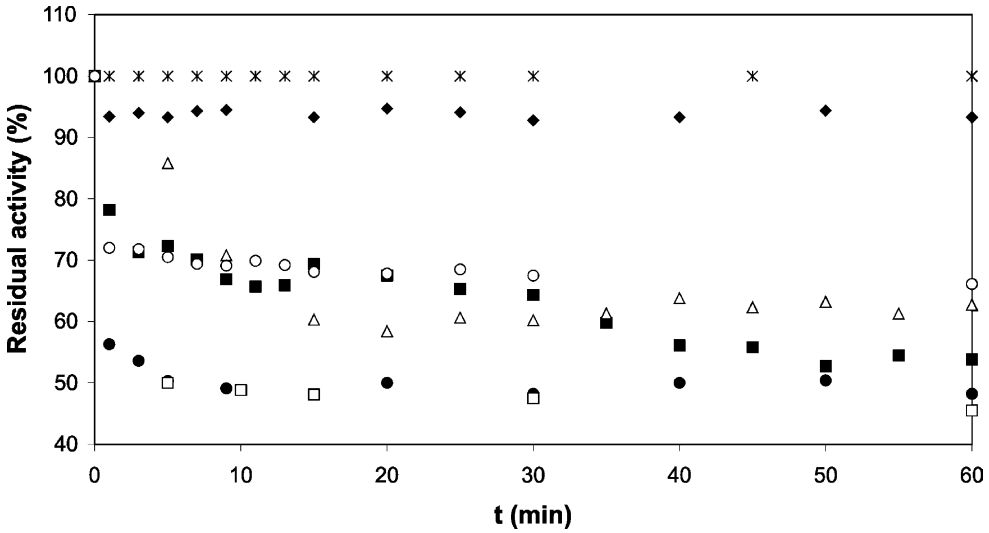

Figure 6. Influence of various proteins on the reversible inactivation of a freshly prepared 50 μg/ml solution of TtxTIM at 80 °C. The time-course of inactivation is shown without additions (■), and in the presence of (200 μg/ml each) GLPDH of *T. tenax* (⋆), GLPDH of *M. thermautotrophicus*, (◆) GAPN of *T. tenax* (△), 1,6-fructosebisphosphat aldolase of *T. tenax* (□), phosphorylating GAPDH of *T. tenax* (○) and hen egg lysozyme (●).

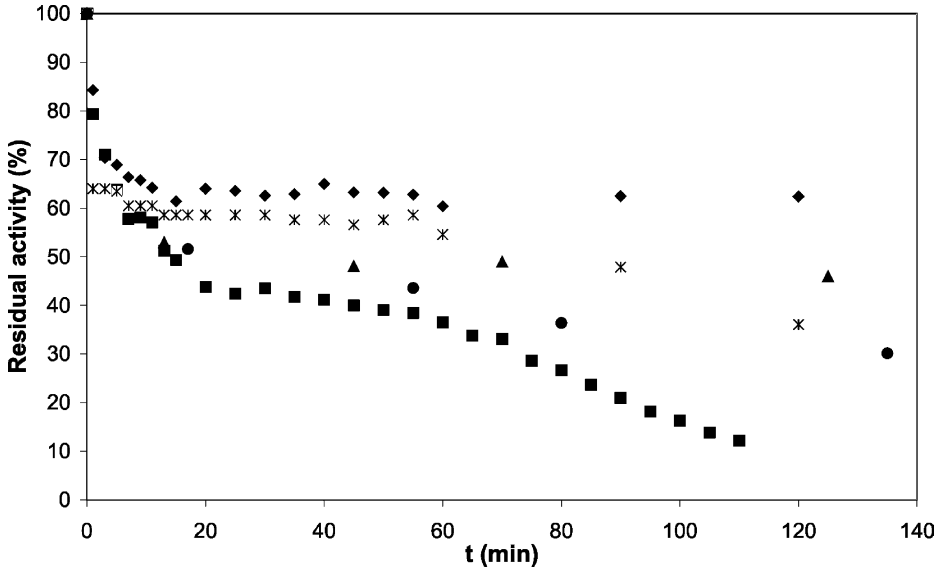

Figure 7. Thermal inactivation of a freshly prepared 50 μg/ml solution of TtxTIM at 92 °C in the absence and in the presence (100 mM each) of various low molecular mass compounds. Control (without additives) (■), trehalose (♦), KCl (●), NH_4SO_4 (▲), cyclic 2,3 diphosphoglycerate (⋆).

number of ion-pairs or ion-pair networks, there are specific regions where electrostatic interactions may be important for thermal stability. TtxTIM has an ion-pair network similar to that of the less thermostable TIMs, responsible for tethering helices 6 and 7 together, a network not found in the more thermostable PwTIM. TtxTIM does not have either of the networks found in helix 4 of PwTIM, which point back into the core of the monomer. These networks possibly serve to stabilize helix 4 in its formation of the tetramer, and may account for some of the differences in the tetrameric association seen in TtxTIM. However, without further experiments to determine the contribution of these networks to the overall thermostability of PwTIM, this cannot be proven. On the other hand, both TtxTIM and PwTIM share a potentially stabilizing ion-pair not seen in any of the other TIMs, tethering the two sections of helix 6 to each other.

The observation that there is a higher proportion of charged surface-exposed area in each of the hyperthermophilic enzymes compared with the less thermostable TIMs, correlates well with previous findings,[12,28] which showed that the surfaces of the hyperthermophilic proteins had an increase in charged residues at the expense of polar residues. These findings reflect the large difference in the proportions of charged *versus* uncharged amino acid residues as deduced from comparisons of complete genomes of mesophiles and hyperthermophiles.[29]

Exposed asparagine and glutamine residues are potential weak points in protein structure, due to their susceptibility to deamidation and cleavage of the peptide bond, especially at temperatures above 90 °C. From that it seems plausible that these weak links are protected or eliminated particularly in hyperthermophilic proteins. As shown in the present study, there is a clear tendency in hyperthermophilic TIMs to reduce these residues from solvent-accessible positions, where such hydrolytic destructions should occur preferentially. On average, the neutralization of these weak points will result in an overall reduction of Asn and Gln in the majority of hyperthermophilic proteins, as deduced by statistical analyses.[28]

Another trend in thermoadaptation of hyperthermophiles is a striking preference for higher oligomeric states in hyperthermophilic proteins. Besides TIM, there are several examples of hyperthermophilic proteins that have a higher oligomeric state than their mesophilic counterparts, e.g. 3-phosphoglycerate kinase[30] or dihydrofolate reductase[31] and aldolases.[32] Experimental data confirm the importance of the additional subunit contacts for the thermal stability of the higher oligomer in some cases.[33–36]

We might assume that the slightly lower thermostability of TtxTIM compared to PwTIM is mainly due to its weaker tetramer association. Although the tetramer interface of TtxTIM is more extensive than that of the more thermostable PwTIM, it is also less hydrophobic, supporting the notion that an increase in hydrophobicity leads to an increase in stability. Many proteins employ an increase in the burial of hydrophobic residues for stabilization. Recent examples include the GAPDH from *M. fervidus*, which has more hydrophobic contacts than mesophilic GAPDHs, facilitated by additional helices,[5] and the alcohol dehydrogenase from *Thermoanaerobacter brockii*, which has more hydrophobic interactions at subunit interfaces than its mesophilic counterparts.[37]

The tetramer contacts are also localised slightly differently in the TtxTIM and PwTIM. In both cases, most of the contacts are contributed by residues in helices 4 and 5; however, TtxTIM has more contacts from loop 4 and the loop following helix 6, while

PwTIM has more contacts from the central areas of the tetramer interface, loop 5, helix 5 and the loop following helix 5. These differences contribute to a looser association of the TxTIM tetramer compared to the PwTIM tetramer.

The question arises as to why *T. tenax* prefers a TIM with a variable dimer/tetramer equilibrium in contrast to the other hyperthermophiles such as *T. maritima*, *M. fervidus* or *P. woesei*, which have very stable tetrameric TIMs. Obviously, *T. tenax* uses other mechanisms for thermostabilising its TIM. Thus, we assume that the observed increased burial of hydrophobic surface area upon formation of the classical TIM dimer in the TtxTIM compared to the PwTIM indicate stronger dimer contacts, which could compensate the weakly stabilizing contacts across the tetramer interface. Extrinsic stabilizing factors such as trehalose, which is present in *T. tenax*, seem to be engaged additionally in protecting the protein against heat-denaturation, as indicated by the protecting effect of the disaccharide against irreversible denaturation at 92 °C.

To begin answering why *T. tenax* does not employ strong tetramer contacts for stabilizing its TIM, we suggest that other factors may compensate and lead to stabilization for physiological reasons. The highly specific influence of the GLPDH of *T. tenax* on the dimer/tetramer equilibrium of TtxTIM, combined with the significantly higher specific activity of TtxTIM (1.5-fold) determined with GLPDH of *T. tenax* as an auxiliary enzyme, clearly indicates a close interaction between TIM and GLPDH with obvious regulatory effects. We therefore suggest that the rapid equilibrium between active tetramers and virtually inactive dimers should sensitize the TtxTIM for internal signals controlling the activity of the enzyme, thus making TtxTIM the first regulated TIM to be described. GLPDH is one candidate for such control, which through its interaction with TIM increases the production of DHAP, possibly leading to an increase in the synthesis of phosphoglycerides. A more favoured hypothesis for explaining the rationale behind this interaction would take the hyperthermophilic environment into account. At high temperatures, there is also the need for sufficient stability of metabolites and intermediates. Several intermediates of the EMP pathway, such as DHAP, GAP, phosphoenolpyruvate and especially 1,3-bisphosphoglycerate, are highly thermolabile and need to be protected against heat-destruction. As shown by previous investigations,[24,25,38,39] the catabolic EMP pathway of *T. tenax* is characterized by significant deviations from the common glycolytic pathway, which are interpreted as thermoadaptive measures to avoid thermolabile intermediates or at least to minimize their intracellular pools and therefore to reduce the velocity of their heat destruction.

The proposed interaction between GLPDH and TIM may be a further modification of the pathway in *T. tenax*, reducing the intracellular pools of labile intermediates of the EMP pathway under anabolic rather than catabolic conditions. Under anabolic conditions, the pathway proceeds, starting with a unidirectional phosphoenolpyruvate synthetase, exclusively *via* reversible enzyme reactions, including phosphorylating GAPDH and 3-phosphoglycerate kinase, which are expressed predominantly under autotrophic conditions.[24] GLPDH seems to be the only enzyme that could effectively adjust the labile intermediates to a lower level through reducing DHAP to the thermostable glycerol 1-phosphate. When considering metabolic thermoadaptation, an acceleration of this reaction by stimulating the GAP/DHAP conversion by TIM under autotrophic conditions is meaningful.

Although we do not understand the structural details and can only argue the functional importance of a TIM/GLPDH interaction, it is reasonable to assume that physiological reasons are responsible for the alternative strategy of thermoadaptation shown by TtxTIM. The example further demonstrates that, due to the balance of stability demands with the individual requirements of function, we cannot expect iron rules for structural thermoadaptation of proteins. Nature seems to be flexible enough to manage appropriate stability by various means. Function, for the most part, dictates the means.

Materials and Methods

Enzyme assay

Activity tests of TIM were performed in both directions, with dihydroxyacetone phosphate (DHAP) or glyceraldehyde 3-phosphate (GAP) as substrate.[38] The assay mixture for standard tests of the DHAP/GAP isomerization (assay temperature 70 °C) contained 90 mM Hepes–KOH (pH 7.3), 10 mM NAD^+, 4 mM DHAP and 7.5 units of recombinant GAPN of *T. tenax*.[38] For the DHAP/GAP isomerisation, different auxiliary enzymes were applied, depending on the assay temperature. At 30–55 °C, glycerol-3-phosphate dehydrogenase from rabbit muscle (Sigma-Aldrich) was applied (1ten units of enzyme, 2 mM GAP, 0.5 mM NADH). For temperatures above 55 °C, the recombinant GLPDH of *M. thermautotrophicus* or *T. tenax* were used (12.5 units of enzyme, 2 mM GAP, 0.5 mM NADPH).

Preparation of the recombinant GLPDH of *M. thermautotrophicus* and *T. tenax*

The recombinant GLPDH of *M. thermautotrophicus* was expressed in *Escherichia coli* BL21-CodonPlus(DE3)-RIL after cloning the *gld* gene from the *M. thermautotrophicus* genome[40] into the expression vector pET 11c, *via* two restriction sites (NdeI and BamHI) introduced by PCR mutagenesis with the primers:

5′CATGGAGAACCATAACATATGGTCACGGTCATTG3′ (sense)

and

5′CGAAATAAACTCCGGATCCCCTAAAATTCGG3′ (antisense)

In the case of GLPDH of *T. tenax*, the coding gene identified in the *T. tenax* genome[41] was amplified with the mutagenic primers:

5′ACAAAATCCATATGAAATTTCTTGAAG3′ (sense)

and

5′GCCGCATGAGCTCATATTAGATG3′ (antisense)

introducing two new restriction sites (NdeI and SacI) and converting the orignal start codon GTG to ATG The fragment was inserted into the pET24A expression vector and expressed in *E. coli* BL21-CodonPlus(DE3)-RIL (Stratagene). Cell-free extracts were heat-precipitated at 80 °C for 30 minutes, centrifuged, dialysed against 50 mM Hepes (pH 7.0) and applied to the assay.

Purification of TIM from *T. tenax* cells

Autotrophically grown *T. tenax* cells (10 g wet weight) were resuspended in buffer A (50 mM Hepes (pH 7.0), 10 mM 2-mercaptoethanol) and disrupted by passing the suspension through a French Press cell at 150 MPa. After centrifugation (at 40,000*g* for 30 minutes), the supernatant was incubated at 80 °C for 30 minutes and centrifuged again. TtxTIM was then precipitated in 40–50% saturated ammonium sulfate. Overnight dialysis was carried out against buffer A at 4 °C, then ammonium sulfate was added to a final concentration of 1.4 M and the protein solution was applied to a phenyl-Sepharose CL-4B column (Pharmacia 30 cm×2.5 cm; flow-rate 0.5 ml/minute) equilibrated with buffer A containing 1.4 M ammonium sulfate. The protein was eluted with a linearly decreasing gradient of ammonium sulfate (1.4–0.0 M) and an increasing gradient of ethylene glycol (0–30%) in a total volume of 400 ml. Fractions with the highest activity were pooled, dialysed against 20 mM sodium phosphate buffer (pH 7.0), 5 mM dithiothreitol, and applied to a Fast Flow hydroxylapatite column (Fluka 25 cm×2 cm; flow-rate 0.2 ml/minute). The protein was eluted by a stepwise increase of the phosphate concentration from 50 to 100 mM. For the final purification, the protein solution was dialysed against buffer A and loaded onto a Red 120-agarose column (Pharmacia 6 cm×1 cm; flow-rate 0.3 ml/minute) equilibrated with the same buffer. After rinsing the column with a sixfold bed volume of buffer A, homogeneous protein was eluted by adding 10 mM sodium phosphate to buffer A. Usually, the recovery from 10 g of cells was 50 μg of protein at a 1700-fold enrichment.

Sequencing of the TxTIM gene, expression of the gene in *E. coli* and purification of the recombinant protein

The TtxTIM gene was identified by Southern hybridization[42] with a nucleotide probe generated by PCR amplification using the degenerated primers 5′ATAAAYTTYAARGCNTAYGG3′ and 5′ATMAAYTCNGGNGGYTC3′ deduced from the heptapepetides INFKAYG of the N-terminal region of the protein (as determined by N-terminal sequencing of the protein) and EPPELIG, a highly conserved sequence region within archaeal TIMs (positions 161–167 in an archaeal consensus alignment).[22] The PCR product comprising 450 bp was cloned in *E. coli* TOP10 using pCR-TOPO 2.1 as the vector. For hybridization, the PCR product was labeled using the DIG High Prime Kit, according to the manufacturer's instructions (Roche). Genomic *T. tenax* DNA prepared as described[43,44] was digested by BamHI and transferred to Biodyne B nylon membranes (Pall) by capillary blotting.[42] Southern hybridisation allowed for the identification of a 3.3 kb BamHI fragment giving a strong hybridization signal, which was selected, cloned and sequenced in both directions.

For expression of the TtxTIM, the coding region was cloned into pJF118EH[45] *via* two new restriction sites (EcoRI and PstI) introduced by PCR mutagenesis with the primers:

5′GGCAGTCCCCGGAATTCACCATGAGGCTTC3′ (sense)

and

5′CCTGAGGCAGCTGCAGTCAGCGGAGCTC3′ (antisense)

To produce TIM, *E. coli* DH5α cells were transformed with the recombinant plasmid The sequence of the expression clone was confirmed by sequencing both strands. For purification, 5 g of recombinant *E. coli* was resuspended in 50 mM Tris–HCl (pH 7.3) containing 30 mM 2-mercaptoethanol. The suspension was passed through a French Press cell (150 MPa) and cell debris was removed by centrifugation (at 50,000*g*, for 30 minutes at 4 °C). After heat-induced precipitation (80 °C, 30 minutes) and centrifugation, the supernatant was dialysed against 50 mM Tris–HCl (pH 7.3), 10 mM 2-mercaptoethanol, then applied to a Red 120-agarose column. Final purification was achieved by gel-filtration using a HiLoad 26/60 Superdex 200 Prep grade column (Pharmacia 60 cm×2.6 cm; room temperature; flow-rate 0.75 ml/minute). Usually, 5 mg of homogeneous protein was isolated from 5 g of *E. coli* cells.

Molecular mass determinations by analytical ultracentrifugation

Sedimentation equilibrium analyses were conducted using an analytical ultracentrifuge Optima X-LA (Beckman Instruments, Palo Alto, CA) equipped with six-channel cells and an AnTi 50 rotor. The protein concentration was varied between 5 μg/ml and 900 μg/ml. Dilutions were performed with 50 mM Hepes–KOH (pH 7.0). Centrifugation was performed at 15,000 rpm at 25 °C. The samples were measured at 230 nm and 280 nm, respectively. The apparent molecular mass M(app) was determined using the software provided by Beckman Instruments. On the basis of the apparent values, the dissociation constant for a dimer/tetramer equilibrium could be calculated according to equation (1):

$$M(\text{app}) = ((c_d D) + (c_t T))/(c_d + c_t) \quad (1)$$

where c_d and c_t are the concentrations of the dimeric and tetrameric forms, respectively. D and T represent the molecular mass of the dimer and tetramer. c_D can be expressed as a function of c_M, and the dissociation constant, K_D:

$$c_D = c_M^2/K_D \quad (2)$$

c_M is a function of the total protein concentration, c_{total}, according to:

$$c_M = -0.5K_D/2 + [(0.5K_D/2)^2 + 0.5K_D c_{total}]^{0.5} \quad (3)$$

Monitoring the influence of protein concentration, temperature, low molecular mass compounds and various proteins on the reversible and irreversible inactivation of TtxTIM

To investigate the influence of extrinsic factors on the activity of the enzyme, TIM solutions (volume 250–500 μl; protein concentration 1–300 μg/ml; buffer 50 mM Hepes–KOH (pH 7.0)) were incubated in the presence and in the absence of various additives at different temperatures (5–92 °C) and the time-course of inactivation was followed by withdrawing aliquots from the incubation mixtures and immediately testing them for enzyme activity. The enzyme assays were performed at 35 °C using rabbit muscle glycerol-3-phosphate dehydrogenase as auxiliary enzyme. To follow the kinetics of reversible and irreversible inactivation, the incubation was started by adding a defined volume of a freshly prepared solution of TIM at a concentration of 0.5 mg/ml (by diluting a 2 mg/ml stock solution kept at 4 °C under N_2 immediately prior to the experiment) to the incubation mixture and the activity was measured over the course of one to two hours.

Crystallisation

Two different crystal forms of TtxTIM were obtained. The first was a hexagonal crystal form, obtained using 10 mg/ml of TtxTIM in 50 mM Hepes–KOH (pH 7.0), 0.3 M KCl, 2 mM DTT, crystallisation conditions 0.1 M Hepes–KOH (pH 7.5), 0.8 M sodium potassium phosphate. The crystals diffracted to 2.5 Å on station X11 at DESY in Hamburg, and belong to spacegroup $P6_522/P6_122$ with cell dimensions $a=b=186.9$ Å, $c=287.8$ Å, $\alpha=\beta=90°$, $\gamma=120°$, suggesting two tetramers in the asymmetric unit with a Matthew's coefficient, $V_M=3.9$ Å^3 Da^{-1}. Molecular replacement using the PwTIM as a phasing model was unsuccessful. A second crystal form was obtained using 10 mg/ml of TtxTIM incubated with 20 mM 2-carboxyethylphosphonic acid (2-CP), a substrate analogue. Orthorhombic crystals with cell dimensions $a=154.1$ Å, $b=91.0$ Å, $c=141.2$ Å, $\alpha=\beta=\gamma=90°$ were obtained in 0.1 M sodium acetate (pH 4.6), 0.2 M ammonium sulfate, with PEG4000 at any concentration between 20% and 30% (w/v). Crystals grew within 48 hours at 20 °C. Cryoprotection of the crystals was achieved by the addition of 15% glycerol to the mother liquor, and they were then flash-frozen at 100K. Data were collected on station BW7A[46] at DESY in Hamburg to 2.3 Å. Data were processed and scaled using DENZO and SCALEPACK.[47] Details of the data collection statistics are given in Table 1.

Structure solution

A molecular replacement solution using the PwTIM structure as a search model was obtained with the orthorhombic data. The unit cell of the orthorhombic crystal form also suggested two tetramers in the asymmetric unit with $V_M=2.65$ Å^3 Da^{-1}. As TtxTIM and PwTIM share a 52% sequence identity, the residues in the PwTIM model were mutated using O[48] to those of the TtxTIM sequence. The rotation function and translation function calculations as implemented in the CNS were used.[49] Using a mutated PwTIM dimer as the search model, and data from 15–4 Å, the top 126 peaks from the rotation function were used to search for a translation function solution. The top solution was fixed and a second translation function search was carried out. The position of the second dimer could be determined only subsequent to pre-translational Patterson correlation refinement, as implemented in CNS, in this case treating each monomer as a rigid body in order to refine the rotation function peaks prior to translation. All domains were subjected to post-translational rigid-body refinement. The same procedure was repeated to search for the third and fourth dimers. The hexagonal crystal form was solved readily by molecular replacement using the refined orthorhombic tetramer structure.

Structure refinement

CNS was used to refine the two tetramers in the orthorhombic asymmetric unit to 2.3 Å. A 10% subset of the data was omitted from all refinement calculations for cross-validation. The *R*-factor dropped to 31.3% and the free *R*-factor to 36.7% after simulated annealing, during which non-crystallographic (NCS) restraints were applied. The NCS restraints were removed and rounds of energy minimisation and individual *B*-factor refinement, and addition of water molecules resulted in a final *R*-factor of 21.5% and *R*-free of 25.9%. The final model is almost complete, with monomers A and B lacking the final three residues, as there was no defined density in these regions. However, monomers D and E are both complete, and the other monomers are lacking only one or two C-terminal residues. The substrate analogue, 2-CP was present in each monomer. The hexagonal crystal form was solved by molecular replacement using the refined orthorhombic model, and refined to 2.5 Å using CNS with NCS restraints maintained throughout, to a final *R*-factor of 19.7% and *R*-free of 22.6%. Each monomer had a phosphate group in the active site, which was present in the crystallisation buffer. Validation with PROCHECK[50] reveals that the overall stereochemistry of both models is good, with the Ramachandran plot showing 98.2% of the residues in the core and allowed regions in the orthorhombic model, and 98.7% in the hexagonal, and 1.3% (orthorhombic) and 0.7% (hexagonal) in generously allowed regions. Both crystal forms have Ala180 in a disallowed region, although the density for this residue is well defined.

Structural analysis

The TIM structures were superimposed on the basis of the three conserved catalytic residues (Lys11, His93, Glu140 in TxTIM numbering) and improved to extend across as many C^α atoms as possible using O. Secondary structure assignment was made using the DSSP software.[51] Exposed surface areas were calculated using the program GRASP.[52] Hydrogen bonds between protein atoms were calculated using HBPLUS,[53] with the default parameters for distances and angles. Ion-pairs were assigned when atoms of opposite charge were found within 4 Å of each other.[54] Interface accessible surface area was calculated through the Protein–Protein Interaction server,[55] using a probe radius of 1.4 Å. Figure 6 was created using BOBSCRIPT[56] and GL_RENDER (L. Esser & J. Deisenhofer, unpublished). Estimation of the susceptibility of a given asparagine or glutamine residue to deamidation was made on the basis of the following two criteria;[57] each of which has two parts, both of which have to be satisfied. The residue may be susceptible if (1i) the side-chain oxygen atom has no hydrogen bond with the $N+1$ peptide nitrogen atom, and (1ii) the C^γ (Asn) or C^δ (Gln) atom points in the right direction for attack by the carboxy peptide nitrogen atom. (2i) There is no steric

hindrance of the formation of a succinimide ring from surrounding side-chains, and (2ii) there is no complex hydrogen bonding network nearby.

Protein Data Bank accession numbers

The coordinates of the orthorhombic and hexagonal crystal form models have been deposited with the RCSB Protein Data Bank with accession numbers 1w0l and 1w0m, respectively.

Acknowledgements

This work was supported, in part, by the award of an EPSRC studentship to H.W. Thanks are due to R. Jaenicke for performing initial ultracentrifugation experiments and for stimulating discussions.

References

1. Walden, H., Bell, G. S., Russell, R. J., Siebers, B., Hensel, R. & Taylor, G. L. (2001). Tiny TIM: a small, tetrameric, hyperthermostable triosephosphate isomerase. *J. Mol. Biol.* **306**, 745–757.
2. Russell, R. J., Hough, D. W., Danson, M. J. & Taylor, G. L. (1994). The crystal structure of citrate synthase from the thermophilic archaeon, *Thermoplasma acidophilum*. *Structure*, **2**, 1157–1167.
3. Russell, R. J., Ferguson, J. M., Hough, D. W., Danson, M. J. & Taylor, G. L. (1997). The crystal structure of citrate synthase from the hyperthermophilic archaeon *Pyrococcus furiosus* at 1.9 Å resolution. *Biochemistry*, **36**, 9983–9994.
4. Maes, D., Zeelen, J. P., Thanki, N., Beaucamp, N., Alvarez, M., Thi, M. H. *et al*. (1999). The crystal structure of triosephosphate isomerase (TIM) from *Thermotoga maritima*: a comparative thermostability structural analysis of ten different TIM structures. *Proteins: Struct. Funct. Genet.* **37**, 441–453.
5. Charron, C., Talfournier, F., Isupov, M. N., Littlechild, J. A., Branlant, G., Vitoux, B. & Aubry, A. (2000). The crystal structure of d-glyceraldehyde-3-phosphate dehydrogenase from the hyperthermophilic archaeon *Methanothermus fervidus* in the presence of NADP(+) at 2.1 Å resolution. *J. Mol. Biol.* **297**, 481–500.
6. Isupov, M. N., Fleming, T. M., Dalby, A. R., Crowhurst, G. S., Bourne, P. C. & Littlechild, J. A. (1999). Crystal structure of the glyceraldehyde-3-phosphate dehydrogenase from the hyperthermophilic archaeon *Sulfolobus solfataricus*. *J. Mol. Biol.* **291**, 651–660.
7. Britton, K. L., Baker, P. J., Borges, K. M. M., Engel, P. C., Pasquo, A., Rice, D. W. *et al*. (1995). Insights into thermal stability from a comparison of the glutamate dehydrogenase from *Pyrococcuc furiosus* and *Thermococcus litoralis*. *Eur. J. Biochem.* **229**, 688–695.
8. Britton, K. L., Yip, K. S., Sedelnikova, S. E., Stillman, T. J., Adams, M. W., Ma, K. *et al*. (1999). Structure determination of the glutamate dehydrogenase from the hyperthermophile *Thermococcus litoralis* and its comparison with that from *Pyrococcus furiosus*. *J. Mol. Biol.* **293**, 1121–1132.
9. Vieille, C. & Zeikus, G. J. (2001). Hyperthermophilic enzymes: sources, uses, and molecular mechanisms for thermostability. *Microbiol. Mol. Biol. Rev.* **65**, 1–43.
10. Jaenicke, R. & Bohm, G. (1998). The stability of proteins in extreme environments. *Curr. Opin. Struct. Biol.* **8**, 738–748.
11. Sterner, R. & Liebl, W. (2001). Thermophilic adaptation of proteins. *Crit. Rev. Biochem. Mol. Biol.* **36**, 39–106.
12. Cambillau, C. & Claverie, J.-M. (2000). Structural and genomic correlates of hyperthermostability. *J. Biol. Chem.* **275**, 32383–32386.
13. Lodi, P. J. & Knowles, J. R. (1991). Neutral imidazole is the electrophile in the reaction catalyzed by triosephosphate isomerase: structural origins and catalytic implications. *Biochemistry*, **30**, 6948–6956.
14. Alvarez, M., Zeelen, J. P., Mainfroid, V., Rentier-Delrue, F., Martial, J. A., Wyns, L. *et al*. (1998). Triosephosphate isomerase (TIM) of the psychrophilic bacterium *Vibrio marinus*. Kinetic and structural properties. *J. Biol. Chem.* **273**, 2199–2206.
15. Banner, D. W., Bloomer, A., Petsko, G. A., Phillips, D. C. & Wilson, I. A. (1976). Atomic coordinates for triose phosphate isomerase from chicken muscle. *Biochem. Biophys. Res. Commun.* **72**, 146–155.
16. Lolis, E., Alber, T., Davenport, R. C., Rose, D., Hartman, F. C. & Petsko, G. A. (1990). Structure of yeast triosephosphate isomerase at 1.9 Å resolution. *Biochemistry*, **29**, 6609–6618.
17. Norledge, B. V., Lambeir, A. M., Abagyan, R. A., Rottmann, A., Fernandez, A. M., Filimonov, V. V. *et al*. (2001). Modeling, mutagenesis, and structural studies on the fully conserved phosphate-binding loop (loop 8) of triosephosphate isomerase: toward a new substrate specificity. *Proteins: Struct. Funct. Genet.* **42**, 383–389.
18. Symersky, J., Li, S., Carson, M. & Luo, M. (2003). Structural genomics of *Caenorhabditis elegans*: triosephosphate isomerase. *Proteins: Struct. Funct. Genet.* **51**, 484–486.
19. Delboni, L. F., Mande, S. C., Rentier-Delrue, F., Mainfroid, V., Turley, S., Vellieux, F. M. *et al*. (1995). Crystal structure of recombinant triosephosphate isomerase from *Bacillus stearothermophilus*. An analysis of potential thermostability factors in six isomerases with known three-dimensional structures points to the importance of hydrophobic interactions. *Protein Sci.* **4**, 2594–2604.
20. Alvarez, M., Wouters, J., Maes, D., Mainfroid, V., Rentier-Delrue, F., Wyns, L. *et al*. (1999). Lys13 plays a crucial role in the functional adaptation of the thermophilic triose-phosphate isomerase from *Bacillus stearothermophilus* to high temperatures. *J. Biol. Chem.* **274**, 19181–19187.
21. Kohlhoff, M., Dahm, A. & Hensel, R. (1996). Tetrameric triosephosphate isomerase from hyperthermophilic Archaea. *FEBS Letters*, **383**, 245–250.
22. Schramm, S., Kohlhoff, M. & Hensel, R. (2001). Triosephosphate isomerase from *Pyrococcus woesei* and *Methanothermus fervidus*. *Methods Enzymol.* **331**, 105–125.
23. Schurig, H., Beaucamp, N., Ostendorp, R., Jaenicke, R., Adler, E. & Knowles, J. R. (1995). Phosphoglycerate kinase and triosephosphate isomerase from the hyperthermophilic bacterium *Thermotoga maritima* form a covalent bifunctional enzyme complex. *EMBO J.* **14**, 442–451.
24. Brunner, N. A., Siebers, B. & Hensel, R. (2001). Role of two different glyceraldehyde-3-phosphate

dehydrogenases in controlling the reversible Embden–Meyerhof–Parnas pathway in *Thermoproteus tenax*: regulation on protein and transcript level. *Extremophiles*, **5**, 101–109.
25. Martins, L.-O., Huber, R., Huber, H., Stetter, K. O., Da Costa, M. & Santos, H. (1997). Organic solutes in hyperthermophilic Archaea. *Appl. Environ. Microbiol.* **63**, 896–902.
26. Hensel, R. & Konig, H. (1988). Thermoadaptation of methanogeneic bacteria by intracellular ion concentration. *FEMS Microbiol. Letters*, **49**, 75–79.
27. Scholz, S., Sonnenbichler, J., Schafer, W. & Hensel, R. (1992). Di-myo-inositol-1,1′-phosphate: a new inositol phosphate isolated from *Pyrococcus woesei*. *FEBS Letters*, **306**, 239–242.
28. Szilagyi, A. & Zavodszky, P. (2000). Structural differences between mesophilic, moderately thermophilic and extremely thermophilic protein subunits: results of a comprehensive survey. *Struct. Fold. Des.* **8**, 493–504.
29. Fukuchi, S. & Nishikawa, K. (2001). Protein surface amino acid compositions distinctively differ between thermophilic and mesophilic bacteria. *J. Mol. Biol.* **309**, 835–843.
30. Hess, D., Kruger, K., Knappik, A., Palm, P. & Hensel, R. (1995). Dimeric 3-phosphoglycerate kinase from hyperthermophilic Archaea; cloning, sequencing and expression of the 3-phosphoglycerate kinase gene of *Pyrococcus woesei* in *Escherichia coli* and characterization of the protein. Structural and functional comparison with the 3-phosphglycerate kinase of *Methanothermus fervidus*. *Eur. J. Biochem.* **233**, 227–237.
31. Dams, T., Auerbach, G., Bader, G., Jacob, U., Ploom, T., Huber, R. & Jaenicke, R. (2000). The crystal structure of dihydrofolate reductase from *Thermotoga maritima*: molecular features of thermostability. *J. Mol. Biol.* **297**, 659–672.
32. Lorentzen, E., Pohl, E., Zwart, P., Stark, A., Russell, R. B., Knura, T. *et al*. (2003). Crystal structure of an archaeal class I aldolase and the evolution of (betaalpha)8 barrel proteins. *J. Biol. Chem.* **278**, 47253–47260.
33. Shima, S., Herault, D. A., Berkessel, A. & Thauer, R. K. (1998). Activation and thermostabilisation effects of cyclic 2,3-diphosphoglycerate on enzymes from the hyperthermophilic *Methanopyrus kandleri*. *Arch. Microbiol.* **170**, 469–472.
34. Shima, S., Thauer, R. K., Ermler, U., Durchschlag, H., Tziatzios, C. & Schubert, D. (2000). A mutation affecting the association equilibrium of formyltransferase from the hyperthermophilic *Methanopyrus kandleri* and its influence on the enzyme's activity and thermostability. *Eur. J. Biochem.* **267**, 6619–6623.
35. Villeret, V., Clantin, B., Tricot, C., Legrain, C., Roovers, M., Stalon, V. *et al*. (1998). The crystal structure of *Pyrococcus furiosus* ornithine carbamoyltransferase reveals a key role for oligomerization in enzyme stability at extremely high temperatures. *Proc. Natl Acad. Sci. USA*, **95**, 2801–2806.
36. Clantin, B., Tricot, C., Lonhienne, T., Stalon, V. & Villeret, V. (2001). Probing the role of oligomerization in the high thermal stability of *Pyrococcus furiosus* ornithine carbamoyltransferase by site-specific mutants. *Eur. J. Biochem.* **268**, 3937–39342.
37. Li, C., Heatwole, J., Soelaiman, S. & Shoham, M. (1999). Crystal structure of a thermophilic alcohol dehydrogenase substrate complex suggests determinants of substrate specificity and thermostability. *Proteins: Struct. Funct. Genet.* **37**, 619–627.
38. Brunner, N. A., Brinkmann, H., Siebers, B. & Hensel, R. (1998). NAD+-dependent glyceraldehyde-3-phosphate dehydrogenase from *Thermoproteus tenax*. The first identified archaeal member of the aldehyde dehydrogenase superfamily is a glycolytic enzyme with unusual regulatory properties. *J. Biol. Chem.* **273**, 6149–6156.
39. Schramm, A., Siebers, B., Tjaden, B., Brinkmann, H. & Hensel, R. (2000). Pyruvate kinase of the hyperthermophilic crenarchaeote *Thermoproteus tenax*: physiological role and phylogenetic aspects. *J. Bacteriol.* **182**, 2001–2009.
40. Smith, D. R., Doucette-Stamm, L. A., Deloughery, C., Lee, H., Dubois, J., Aldredge, T. *et al*. (1997). Complete genome sequence of *Methanobacterium thermoautotrophicum* deltaH: functional analysis and comparative genomics. *J. Bacteriol.* **179**, 7135–7155.
41. Siebers, B., Tjaden, B., Michalke, K., Gordon, P., Sensen, C. W., Zibat, A. *et al*. (2004). Reconstruction of the carbohydrate metabolism of *Thermoproteus tenax* using genomic and biochemical data. *J. Bacteriol.* **186**, 2179–2194.
42. Southern, E. M. (1975). Detection of specific sequences among DNA fragments separated by gel electrophoresis. *J. Mol. Biol.* **98**, 503–517.
43. Weil, C. F., Cram, D. S., Sherf, B. A. & Reeve, J. N. (1988). Structure and comparative analysis of the genes encoding component C of methyl coenzyme M reductase in the extremely thermophilic archaebacterium *Methanothermus fervidus*. *J. Bacteriol.* **170**, 4718–4726.
44. Meakin, S., Nash, J., Murray, W., Kennedy, K. & Sportt, G. (1991). A generally applicable technique for the extraction of restrictable DNA from methanogenic bacteria. *J. Microbiol. Methods*, **14**, 119–126.
45. Furste, J. P., Pansegrau, W., Frank, R., Blocker, H., Scholz, P., Bagdasarian, M. & Lanka, E. (1986). Molecular cloning of the plasmid RP4 primase region in a multi-host-range tacP expression vector. *Gene.* **48**, 119–131.
46. Pohl, E., Gonzalez, A., Hermes, C. & van Silfhout, R. G. (2001). Overview of the tunable beamlines for protein crystallography at the EMBL Hamburg Outstation; an analysis of current and future usage and developments. *J. Synchrotron Radiat.* **8**, 1113–1120.
47. Otwinowski, Z. & Minor, W. (1997). Processing of X-ray diffraction data collected in oscillation mode. *Methods Enzymol.* **276**, 307–326.
48. Jones, T. A., Zou, J. Y., Cowan, S. W. & Kjeldaaard, M. (1991). Improved methods for builiding protein models in electron density maps and the location of errors in these models. *Acta Crystallog. sect. A*, **47**, 110–119.
49. Brunger, A. T., Adams, P. D., Clore, G. M., DeLano, W. L., Gros, P., Grosse-Kuntsleve, R. W. *et al*. (1998). Crystallography and NMR system (CNS): a new software package for macromolecular structure determination. *Acta Crystallog. sect. D*, **54**, 905–921.
50. Laskowski, R. A., MacArthur, M. W., Moss, D. S. & Thornton, J. M. (1993). PROCHECK: a program to check stereochemical quality of protein structures. *J. Appl. Crystallog.* **26**, 283–291.
51. Kabsch, W. & Sander, C. (1983). Dictionary of protein secondary structure: pattern recognition of hydrogen-bonded and geometrical features. *Biopolymers*, **22**, 2577–2637.

52. Nichols, A., Sharp, K. A. & Honig, B. (1991). Protein folding and association: insights from the interfacial and thermodynamic properties of hydrocarbons. *Proteins: Struct. Funct. Genet.* **11**, 281–296.
53. McDonald, I. K. & Thornton, J. M. (1994). Satisfying hydrogen-bonding potential in proteins. *J. Mol. Biol.* **238**, 777–793.
54. Barlow, D. J. & Thornton, J. M. (1983). Ion pairs in proteins. *J. Mol. Biol.* **168**, 867.
55. Jones, S. & Thornton, J. M. (1996). Principles of protein–protein interactions derived from structural studies. *Proc. Natl Acad. Sci. USA*, **93**, 13–20.
56. Esnouf, R. M. (1997). BOBSCRIPT: an extensively modified version of MOLSCRIPT that includes greatly enhanced coloring capabilities. *J. Mol. Graph. Model.* **15**, 132–143.
57. Daniel, R. M., Dines, M. & Petach, H. H. (1996). The denaturation and degradation of stable enzymes at high temperatures. *Biochem. J.* **317**, 1–11.

Edited by J. Thornton

(Received 12 January 2004; received in revised form 28 June 2004; accepted 8 July 2004)